Co-published by
Institute of Fluid-Flow Machinery
Polish Academy of Sciences
Committee on Thermodynamics and Combustion
Polish Academy of Sciences

http://www.imp.gda.pl/archives-of-thermodynamics/

Soret and Dufour effects on an unsteady MHD flow about a permeable rotating vertical cone with variable fluid properties

Temjennaro Jamir[a*], Hemanta Konwar[a]

[a]Kohima Science College, Jotsoma, Kohima 797001, India
*Corresponding author email: temjennarojamir.tj@gmail.com

Received: 05.08.2023; revised: 30.08.2023; accepted: 12.10.2023

Abstract

The objective of the present work is to examine the characteristics of unsteady incompressible magnetohydrodynamic fluid flow around a permeable rotating vertical cone. The effects of thermal radiation, viscous dissipation, and the Soret and Dufour effects are investigated in the analysis of heat and mass transfer. The viscosity of the fluid is considered inversely proportional to the temperature, and the thermal conductivity of the fluid is considered directly proportional to the temperature. The governing equations are converted into ordinary differential equations using suitable similarity transformations, which are then solved numerically using bvp4c from MATLAB. Results obtained in this study are in excellent correlation with previously conducted studies. The results demonstrate that the Dufour and Soret effects subsequently reduce the heat transit rate (by –3.3%) and mass transit rate (by –1.2%) of the system. It is also detected that fluids with higher viscosity tend to increase tangential skin friction (+8.9%) and azimuthal skin friction (+8.3%). The heat transit rate of the system is found to be more efficient for fluids with higher viscosity and lower thermal conductivity and Eckert numbers. Furthermore, the thickness of the momentum, thermal, and concentration boundary layers significantly reduces while the heat and mass transit rates (+17.8% and +18.3%, respectively) of the system become more efficient for greater values of the unsteadiness parameter.

Keywords: Rotating cone; Temperature-dependent viscosity; Temperature-dependent thermal conductivity; Viscous dissipation, Soret and Dufour effects

Vol. 45(2024), No. 1, 75–86; doi: 10.24425/ather.2024.150440

Cite this manuscript as: Jamir, T, & Konwar, H. (2024). Soret and Dufour effects on an unsteady MHD flow about a permeable rotating vertical cone with variable fluid properties. *Archives of Thermodynamics*, 45(1), 75–86.

1. Introduction

In a variety of applications and industrial processes, both heat and mass transfer are crucial. The equipment, such as gas turbines, various missile propulsion systems, space vehicles, satellites, nuclear reactors, and aircraft, extensively relies on double-diffusive mixed convection over rotating bodies [1].

Hering and Grosh [2] investigated laminar flow across a non-isothermal cone. Sparrow and Cess [3] investigated an axial magnetic field effect on flow and heat transfer over a revolving disc. A steady free convective flow along a vertical cone and a wedge under the influence of transverse magnetic field was presented by Chamkha [4]. Takhar et al. [5] discovered that when an axi-symmetric body spins in a forced flow field, the centrifugal force causes the fluid at the body surface to move outward in the radial direction.

Nomenclature

a^* – mean absorption coefficient
B_0 – magnetic field, T
C – species concentration, kg/m^3
C_{fy} – azimuthal skin friction
C_{fx} – tangential skin friction
C_0 – reference concentration
c_p – specific heat at constant pressure, J/(kgK)
C_w – sheet concentration
C_∞ – free stream concentration, kg/m^3
c_s – concentration susceptibility
Du – Dufour number, $= \frac{D_m K_T}{c_s c_p \nu_\infty}\left(\frac{C_w - C_\infty}{T_w - T_\infty}\right)$
D_m – mass diffusivity, m^2/s
Ec – Eckert number, $= \frac{xL\Omega^2 sin^2\alpha}{c_p(T_0 - T_\infty)}$
f_w – dimensionless suction/injection
$f(\eta)$– normal velocity component
$-f'(\eta)$ – tangential velocity component
g – acceleration due to gravity, m/s^2
$g(\eta)$ – azimuthal velocity component
Gr$_L$ – thermal Grashof number, $= g\beta_T cos\alpha(T_0 - T_\infty)\frac{L^3}{{\nu_\infty}^2}$
Hα^2 – square of Hartmann number, $= \frac{\sigma {B_0}^2 L^2(1-st^*)}{\mu_\infty}$
K_T – thermal diffusion ratio, kg/m^3
$k(T)$ thermal conductivity, W/(mK)
k_∞ – constant thermal conductivity
L – characteristic length, m
M – magnetic parameter, $= \frac{\mathrm{Ha}^2}{\mathrm{Re}_L}$
N – Buoyancy ratio, $= \frac{\beta_C(C_w - C_\infty)}{\beta_T(T_w - T_\infty)}$
Pr – Prandtl number, $= \frac{\mu_\infty c_p}{k_\infty}$
Rd – radiation, $= \frac{k_\infty a^*}{4\sigma^* T_\infty^3}$
Ri – Richardson number, $= \frac{\mathrm{Gr}_L}{{\mathrm{Re}_L}^2}$
Re$_L$ – Reynolds number, $= \frac{\Omega L^2 sin\alpha}{\nu_\infty}$
Re$_x$ – local Reynolds number, $= \frac{\Omega x^2 sin\alpha}{\nu_\infty(1-st^*)}$
Sc – Schmidt number, $= \frac{\nu_\infty}{D_m}$
Sr – Soret number, $= \frac{D_m K_T}{T_m \nu_\infty}\left(\frac{T_w - T_\infty}{C_w - C_\infty}\right)$
s – unsteadiness parameter
t^* – dimensionless time
t – time, s
T – fluid temperature, K
T_m – mean fluid temperature, K
T_w – sheet temperature, K
T_∞ – free stream temperature, K
T_0 – reference temperature, K
$\boldsymbol{V}$ – velocity vector
u, v, w – velocity along tangential, circumferential, normal direction respectively, m/s
w_0 – suction velocity, m/s
x, y, z – curvilinear coordinate, m

Greek Symbols

β_T, β_C – coefficients of thermal and mass expansion, K, kg
μ – dynamic viscosity, kg/(ms)
σ^* – Stefan Boltzmann constant, W/(m^{2}K^4)
μ_∞ – ambient fluid dynamic viscosity, kg/(ms)
ν – kinematic viscosity, m^2/s
$\phi(\eta)$ – dimensionless concentration
ν_∞ – kinematic viscosity of ambient fluid, m^2/s
$\theta(\eta)$ dimensionless temperature
ρ_∞ – constant fluid density, kg/m^3
Ω – angular velocity, 1/s
σ – electric conductivity, s/m
η – dimensionless variable, m
δ – temperature dependent viscosity, m^2/s
ε – temperature dependent thermal conductivity, W/(mK)
α – semi vertical angle, rad

The research mentioned above dealt with steady flows. For laminar flow across a vertical cone in a steady state for two-dimensional axi-symmetric issues, several authors identified comparable solutions. Because the spinning body's angular velocity varies over time or fluctuates abruptly in many real-life situations, the flow may be unstable. Ece [6] looked into the unsteady flow of a rotating symmetric body that is impulsively translating and spinning and established a solution. Chamkha and Al-Mudhaf [7] also analysed this unsteady fluid flow behaviour over a conical surface with heat generation/absorption, Anilkumar and Roy [8] took into account an unsteady rotating cone to analyse the flow of a rotating fluid. A study on mixed convection nanofluid flow past a vertical wedge was presented in the study conducted by Gorla et al. [9], the study concluded that upon enlarging the wedge angle the heat and mass transit rates could be improved. Another study on the flow across a cone/wedge for an Oldroyd-B fluid was considered in the study conducted by Reddy et al.[10]. Further, Reddy et al.[11] estimated non-linear thermal radiative nanofluid steady flow over a rotating cone and Saleem [12] accounted for third-grade fluid flow properties for a rotating cone. A study on water-based nanofluid through a conical surface with single and multi-wall carbon nanotubes was considered by Shah et al. [13]. Krishna et al. [14] presented an analysis of an unsteady magnetohydrodynamic (MHD) non-Newtonian flow over an exponentially accelerated surface under the influence of slip velocity in a rotating frame. The study showed that the presences of the rotation parameter significantly reduce the fluid primary velocity.

Furthermore, the Soret and Dufour effects were overlooked in all previous studies. When density variations occur in the flow regime, such impacts are considerable. In binary fluid mixtures, the Soret and Dufour effects are crucial, and are frequently found in the field of separation processes. When a species with a lower density than the ambient fluid is introduced in a fluid domain, Soret and Dufour impacts might become prominent. The Soret effect has been commonly used to separate isotopes in mixtures of extremely low molecular weight gases like hydrogen and helium, meanwhile, the Dufour effect has been shown to be beneficial for the separation of medium molecular weight gases like nitrogen and air. It has varied applications in the vapour deposition process for optical fibre fabrication, cooling applications, heat exchangers, steel industries, and to separate distinct polymers. These properties have been studied by Chamkha and Rashad [15] who considered unsteady fluid flow

for a rotating vertical cone with Soret and Dufour effect. Krishna et al. [16] accounted for rotating mixed convection flow past an infinite vertical plate to study the influence of the Soret effect, it was concluded that the Soret number promotes the concentration distribution. An analysis of the Soret and Dufour effects for fluid exhibiting relaxation/retardation time effect was performed by Yasir et al. [17] and Reddy [18] who considered Oldroyd-B liquid flow across a cone/wedge under the effects of Soret and Dufour. Saleem [19] accounted for Walter's B nanofluid flow about a rotating cone with the effect of Soret and Dufour. Taking into consideration the multi slip effect, Nadeem et al. [20] accounted for unsteady micropolar fluid flow over an exponential sheet under the influence of the thermophoretic effects. The study showed that for higher values of the thermophoresis parameter the temperature profile improved. Furthermore, this effect of Soret and Dufour was considered in studies conducted by Khan et al. [21] and Ghoneim [22].

Variations in viscosity and thermal conductivity affect the velocity and temperature profiles, resulting in various heat and mass transfer coefficients. However, these characteristics in each of the investigations listed above were deemed to be constant. Moreover, the temperature is known to affect fluid viscosity and thermal conductivity; for instance, Abd El-Aziz [23] considers water's absolute viscosity which reduces by 240% when temperatures increase from 10°C (μ = 0.0131 gcm^{-1}s^{-1}) to 50°C (μ = 0.00548 gcm^{-1}s^{-1}). In order to effectively anticipate flow behaviour, these variations in viscosity and thermal conductivity must be considered. Lai and Kulacki [24] took into account variable viscosity for a moving flat plate, while Prasad et al. [25] considered variable fluid properties for a stretching sheet. Mukhopadhyay [26] in his study considered variable viscosity and thermal conductivity for a porous stretching sheet. Khan et al. [27] accounted for micropolar fluid flow to study the temperature dependent fluid properties to analyse the heat transfer rate and flow properties. The study concluded that the variability in transport properties led to a rise in heat transfer and a decrease in skin friction. In another exploration Khan and Nadeem [28] presented a comparative study to understand the influence of the thermophoretic effects and the variable thermal conductivity on a linear/exponential stretching sheet using the bvp4c numerical technique. Further, Ahmad et al. [29] considered three dimensional bioconvective flow to analyse variable thermal conductivity over an exponentially stretching sheet.

The temperature distributions are altered by viscous dissipation, which acts as an energy source and has an impact on heat transfer rates. Whether the cone is being heated or cooled affects the significance of viscous dissipation. Malik et al. [30] accounted for fluid flow over a rotating cone to analyse the influence of viscous dissipation on the mixed convective fluid flow, the study revealed that the higher Eckert number promotes the heat transfer rate. Sambath et al. [31] conducted a numerical study of the effect of viscous dissipation on a chemically reacting MHD flow over a vertical cone. Also, dissipative MHD nanofluid flow past a vertical cone was taken into consideration in the study conducted by Ragulkumar et al. [32]. Further, Khan et al. [33] accounted for ternary nanomaterials to analyse the thermal conductivity performance with dissipation.

The preceding discussions have highlighted the significant influence of viscous dissipation, temperature-dependent viscosity and thermal conductivity, as well as the Soret and Dufour effects, on heat and mass transfer phenomena. However, additional investigation is necessary to examine the combined effect of these variables on the flow, heat and mass transfer in an unsteady mixed convection flow about a rotating vertical cone. To the best of the authors' knowledge, this issue is yet to be explored. The innovative aspect of the present model is the investigation of the unsteady MHD fluid flow across the rotating vertical cone while taking into consideration the temperature-dependent viscosity and thermal conductivity together with viscous dissipation and the Soret and Dufour effects. The purpose of this study is to provide a comprehensive understanding of the key parameters that influence the characteristics of momentum, thermal and concentration boundary layers, as well as the parameters that are of particular significance in engineering applications. The findings of this study have significant implications for the development and production of cone-shaped materials used in rotating condensers for seawater distillation, nuclear plants, thermal systems, rotating heat exchangers, space aircraft, and oil and gas industries, etc. The methodology employed in this work involves the application of appropriate similarity transformations to transform the governing system of equations into a solvable form. These transformed equations are subsequently solved using MATLAB's bvp4c solver to generate precise numerical solutions.

2. Mathematical formulation

Consider an unsteady, laminar, incompressible, axi-symmetric, electrically conducting and radiative fluid flow about a permeable vertical rotating cone in an ambient fluid with uniform angular velocity Ω. The cone surface has been estimated to have homogeneous fluid suction/injection with velocity w_0, and the viscosity and thermal conductivity of the fluid are deemed to be temperature dependent. The rectangular coordinate system (x, y, z) has been used, in which the *x*-axis is taken along the tangential direction, the *y*-axis is taken along a circular section, and the *z*-axis is normal to the cone, as shown in Fig. 1.

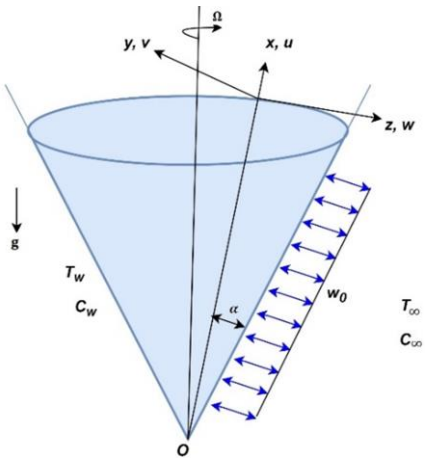

Fig. 1. Physical model and coordinate system.

The velocity components in the tangential, azimuthal and normal directions are taken as u, v and w respectively. In the normal direction, a homogeneous magnetic field of strength B_0 is applied. The ambient temperature T_∞ and concentration C_∞ are assumed to be constant, whereas the wall temperature T_w and wall concentration C_w are defined as $T_w = T_\infty + \frac{T_0 - T_\infty}{(1-st^*)^2}\left(\frac{x}{L}\right)$ and $C_w = C_\infty + \frac{C_0 - C_\infty}{(1-st^*)^2}\left(\frac{x}{L}\right)$. It is supposed that the surface of the cone is electrically insulated, and it is also expected that the magnetic Reynolds number is negligible. In this particular instance, it is feasible to disregard the induced magnetic field when comparing it to the applied magnetic field. In the absence of any applied or polarization voltage within the flow field, the electric field $\vec{E} = 0$. Therefore, the Navier-Stokes equations and Maxwell's equations are decoupled, and in the absence of the magnetic dissipation, the hall and ion slip effects, the only influence of the magnetic field is due to the Lorentz force [34]. The vector form of the governing equations is given below (Gnaneswara Reddy et al. [11]):

Conservation of mass:

$$\nabla . \boldsymbol{V} = 0 \, . \tag{1}$$

Conservation of momentum:

$$\rho_\infty \left(\frac{\partial u}{\partial t} + \boldsymbol{V}.\nabla u - \frac{v^2}{x}\right) = -\nabla p + \nabla(\mu(T)\nabla u) + g\rho_\infty[\beta_T(T - T_\infty) + \beta_C(C - C_\infty)]cos\alpha - \sigma {B_o}^2 u \, , \tag{2}$$

$$\rho_\infty \left(\frac{\partial v}{\partial t} + \boldsymbol{V}.\nabla v + \frac{uv}{x}\right) = -\nabla p + \nabla(\mu(T)\nabla v) - \sigma {B_o}^2 v \, . \tag{3}$$

Conservation of energy:

$$\rho_\infty c_p \left(\frac{\partial T}{\partial t} + \boldsymbol{V}.\nabla T\right) = \nabla(k(T)\nabla T) - \nabla q_r + \frac{D_m K_T \rho_\infty}{c_s}\nabla^2 C + \mu(T)(\nabla \boldsymbol{V}.\nabla \boldsymbol{V}). \tag{4}$$

Conservation of species:

$$\frac{\partial C}{\partial t} + \boldsymbol{V}.\nabla C = D_m \nabla^2 C + \frac{D_m K_T}{T_m}\nabla^2 T \tag{5}$$

Under the hypotheses stated above and using Boussinesq's approximation, Eqs. (1)–(5) reduce to (Tien and Tsuji [1], Chamkha and Al-Mudhaf [7], Saleem et al. [19]):

$$\frac{\partial u}{\partial x} + \frac{u}{x} + \frac{\partial w}{\partial z} = 0, \tag{6}$$

$$\frac{\partial u}{\partial t} + u\frac{\partial u}{\partial x} + w\frac{\partial u}{\partial z} - \frac{v^2}{x} = \frac{1}{\rho_\infty}\frac{\partial}{\partial z}\left(\mu(T)\frac{\partial u}{\partial z}\right) + g[\beta_T(T - T_\infty) + \beta_C(C - C_\infty)]cos\alpha - \frac{\sigma {B_o}^2}{\rho_\infty}u \, , \tag{7}$$

$$\frac{\partial v}{\partial t} + u\frac{\partial v}{\partial x} + w\frac{\partial v}{\partial z} + \frac{uv}{x} = \frac{1}{\rho_\infty}\frac{\partial}{\partial z}\left(\mu(T)\frac{\partial v}{\partial z}\right) - \frac{\sigma {B_o}^2}{\rho_\infty}v \, , \tag{8}$$

$$\frac{\partial T}{\partial t} + u\frac{\partial T}{\partial x} + w\frac{\partial T}{\partial z} = \frac{1}{\rho_\infty c_p}\frac{\partial}{\partial z}\left(k(T)\frac{\partial T}{\partial z}\right) - \frac{1}{\rho_\infty c_p}\frac{\partial q_r}{\partial z} + \frac{D_m K_T}{c_s c_p}\frac{\partial^2 C}{\partial z^2} + \frac{\mu(T)}{\rho_\infty c_p}\left\{\left(\frac{\partial u}{\partial z}\right)^2 + \left(\frac{\partial v}{\partial z}\right)^2\right\}, \tag{9}$$

$$\frac{\partial C}{\partial t} + u\frac{\partial C}{\partial x} + w\frac{\partial C}{\partial z} = D_m\frac{\partial^2 C}{\partial z^2} + \frac{D_m K_T}{T_m}\frac{\partial^2 T}{\partial z^2} \, . \tag{10}$$

The boundary conditions for the problem are (Chamkha and Al-Mudhaf [7], Saleem et al. [19]):

$$\begin{gathered} u(x,0,t) = 0, \quad v(x,0,t) = \frac{\Omega x sin\alpha}{(1-st^*)}, \quad w(x,0,t) = w_0 \, , \\ T(x,0,t) = T_w(x), \quad C(x,0,t) = C_w(x) \, , \\ u(x,\infty,t) = v(x,\infty,t) = 0, \quad T(x,\infty,t) = T_\infty, \\ C(x,\infty,t) = C_\infty \, . \end{gathered} \tag{11}$$

The radiative heat flux $\frac{\partial q_r}{\partial z}$ in Eq. (9) is simplified using the Rosseland approximation given by (Brewster [35]):

$$q_r = -\frac{4\sigma^*}{3a^*}\frac{\partial T^4}{\partial z} \, . \tag{12}$$

Because the temperature difference within the flow is very minimal, higher-order terms with a degree greater than one are ignored in $T - T_\infty$. By escalating T^4 into the Taylor series around T_∞, the linear structure of Eq. (12) can be obtained:

$$T^4 \approx 4T_\infty^3 T - 3T_\infty^4 \, . \tag{13}$$

Thus,

$$\frac{\partial q_r}{\partial z} = -\frac{16\sigma^* T_\infty^3}{3a^*}\frac{\partial^2 T}{\partial z^2} \, . \tag{14}$$

Additionally, the fluid viscosity is considered to vary as an inverse linear function of temperature ((Prasad et al. [25]):

$$\mu(T) = \frac{\mu_\infty}{1+\gamma(T-T_\infty)} = \frac{\mu_\infty}{1+\delta\theta} \, . \tag{15}$$

The variation of thermal conductivity is expressed as (Mukhopadhyay [26]):

$$k(T) = k_\infty\,(1 + b(T - T_\infty) = k_\infty(1 + \varepsilon\theta)\,, \qquad (16)$$

where $\delta = \gamma(T_w - T_\infty)$ is the viscosity parameter such that $\delta > 0$ for liquid, $\delta < 0$ for gas, and $\varepsilon = b(T_w - T_\infty)$ is the thermal conductivity parameter such that $b > 0$ for fluids like water and air while $b < 0$ for lubricating oil. The range of possibilities for ε is as follows: $0 \le \varepsilon \le 0.12$ for water, $0 \le \varepsilon \le 6$ for air, and $-0.1 \le \varepsilon \le 0$ for lubricating oils (Hermann, Schlichting and Gersten [36]). The viscosity parameter δ will be treated as negative and the thermal conductivity parameter ε as positive in the current problem for numerical computation. The following is the relation between the viscosity and temperature of water and air, which are the most commonly utilized fluids in industries (Lai and Kulacki [24]):

– based on T_∞ = 288 K (15°C); $1/\mu = 29{,}83(T - 258{,}6)$ for water,
– based on T_∞ = 293 K (20°C); $1/\mu = -123{,}2(T - 742{,}6)$ for air.

The following transformations can be used to convert Eqs. (6)–(10) into non-linear dimensionless ordinary differential equations (Anilkumar and Roy [8], Saleem [19], Chamkha and Rashad [15]):

$$\eta = \left(\frac{\Omega\sin\alpha}{\nu_\infty(1-st^*)}\right)^{\frac{1}{2}} z, \quad t^* = (\Omega\sin\alpha)t,$$
$$u = -\frac{\Omega x\sin\alpha}{2(1-st^*)} f'(\eta), \quad v = \frac{\Omega x\sin\alpha}{(1-st^*)} g(\eta), \qquad (17)$$
$$w = \left(\frac{\Omega\nu_\infty sin\alpha}{1-st^*}\right)^{\frac{1}{2}} f(\eta), \;\; T = T_\infty + (T_w - T_\infty)\theta(\eta),$$
$$C = C_\infty + (C_w - C_\infty)\phi(\eta)$$

With the above transformations Eq. (6) is satisfied identically and Eqs. (7)–(10) are obtained as follows (Eqs. (18)–(21)):

$$f''' - (1+\delta\theta)\left\{ s\left(f' + \frac{\eta}{2}f''\right) - \frac{f'^2}{2} + ff'' + 2g^2 + \frac{\delta}{(1+\delta\theta)^2}\theta' f'' + 2\mathrm{Ri}(\theta + N\phi) + Mf'\right\} = 0\,, \qquad (18)$$

$$g'' - (1+\delta\theta)\left\{ s\left(g + \frac{\eta}{2}\,g'\right) - f'g + fg' + \frac{\delta}{(1+\delta\theta)^2}\theta' g' + Mg\right\} = 0\,, \qquad (19)$$

$$\theta'' - \left\{\frac{1}{\mathrm{Pr}}\left(1 + \varepsilon\theta + \frac{4}{3Rd}\right)\right\}^{-1}\left\{ s\left(\frac{\eta}{2}\theta' + 2\theta\right) + f\theta' - \frac{1}{2}f'\theta - \frac{1}{\mathrm{Pr}}\varepsilon\theta'^2 - \frac{\mathrm{Ec}}{1+\delta\theta}\left(\frac{1}{4}f''^2 + g'^2\right) - \mathrm{Du}\,\phi''\right\} = 0\,, \qquad (20)$$

$$\phi'' + \mathrm{Sc}\left\{\frac{1}{2}f'\phi - f\phi' - s\left(\frac{\eta}{2}\phi' + 2\phi\right) + \mathrm{Sr}\,\theta''\right\} = 0\,, \qquad (21)$$

with the following boundary conditions:

– at η =0:

$$f(\eta) = f_w, \quad f'(\eta) = 0, \quad g(\eta) = 1, \quad \theta(\eta) = 1, \quad \phi(\eta) = 1, \qquad (22a)$$

– as $\eta \to \infty$:

$$f'(\eta) = g(\eta) = \theta(\eta) = \phi(\eta) = 0. \qquad (22b)$$

Here prime represents differentiation with respect to η and suction/injection velocity $f_w = w_0\sqrt{\frac{1-st^*}{\Omega\nu_\infty\sin\alpha}}$ is such that $f_w < 0$ indicates suction, $f_w = 0$ indicates impermeable rotating cone, and $f_w > 0$ indicates injection.

The parameters of engineering importance, i.e. skin friction coefficients, Nusselt number, and Sherwood numbers are defined as follows:

$$C_{fx} = \frac{2\mu(T)\left(\frac{\partial u}{\partial z}\right)_{z=0}}{\rho_\infty\left(\frac{\Omega x\sin\alpha}{1-st^*}\right)^2} = -\frac{\mathrm{Re}_x^{-1/2} f''(0)}{(1+\delta\theta)} \qquad (23)$$

$$C_{fy} = \frac{-2\mu(T)\left(\frac{\partial v}{\partial z}\right)_{z=0}}{\rho_\infty\left(\frac{\Omega x\sin\alpha}{1-st^*}\right)^2} = -\frac{2\mathrm{Re}_x^{-1/2} g'(0)}{(1+\delta\theta)} \qquad (24)$$

$$\mathrm{Nu}_x = \frac{-x\left\{k(T) + \frac{16\sigma^* T_\infty^3}{3a^*}\right\}\left(\frac{\partial T}{\partial z}\right)_{z=0}}{k_\infty(T_W - T_\infty)} = -\mathrm{Re}_x^{\frac{1}{2}}(1 + \varepsilon + \frac{4}{3Rd})\theta'(0) \qquad (25)$$

$$\mathrm{Sh}_x = \frac{-xD_m\left(\frac{\partial C}{\partial z}\right)_{z=0}}{D_m(C_w - C_\infty)} = -\mathrm{Re}_x^{1/2}\phi'(0) \qquad (26)$$

3. Numerical method for solution

The system of ordinary differential equations Eqs. (18)–(21) subject to the boundary conditions Eqs. (22a) and (22b) is turned into a system of first-order ordinary differential equations and then solved using MATLAB's built-in solver bvp4c (Shampine et al. [37]) with some initial guesses to yield numerical results. The process is shown below:

– Assume:

$$f = y_1\,, \quad f' = y_2\,, \quad f'' = y_3\,, \quad g = y_4\,, \quad ,g' = y_5\,, \qquad (27)$$
$$\theta = y_6\,, \quad \theta' = y_7\,, \quad \phi = y_8\,, \quad \phi' = y_9\,.$$

– Using Eq. (27) in the Eqs. (18)–(21), the following systems of first-order equations are obtained:

$$y_1' = y_2 \qquad (28)$$

$$y_2' = y_3 \qquad (29)$$

$$y_3' = (1+\delta y_6)\left[s\left(y_2 + \frac{\eta}{2}y_3\right) - \frac{1}{2}y_2^2 + y_1y_3 + 2y_4^2 + \frac{\delta}{(1+\delta y_6)^2}y_7y_3 + 2\mathrm{Ri}(y_6 + Ny_8) + My_2\right], \qquad (30)$$

$$y_3' = (1+\delta y_6)\left[s\left(y_2 + \frac{\eta}{2}y_3\right) - \frac{1}{2}y_2^2 + y_1y_3 + 2y_4^2 + \frac{\delta}{(1+\delta y_6)^2}y_7y_3 + 2\mathrm{Ri}(y_6 + Ny_8) + My_2\right], \qquad (30)$$

$$y_4' = y_5\,, \tag{31}$$

$$y_5' = (1+\delta y_6)\left[s\left(y_4+\frac{\eta}{2}y_5\right) - y_2y_4 + y_1y_5 + \frac{\delta}{(1+\delta y_6)^2}y_7y_5 + My_4\right], \tag{32}$$

$$y_6' = y_7\,, \tag{33}$$

$$y_7' = \frac{3Rd\mathrm{Pr}}{3Rd(1+\varepsilon y(6)-\mathrm{PrSrScDu})+4}\left[2s(y_6-\mathrm{DuScy}_8)+\frac{\eta s}{2}(y_7-\mathrm{DuScy}_9)+\frac{1}{2}y_2(\mathrm{DuScy}_8-y_6)+y_1(y_7-\mathrm{DuScy}_9)-\frac{1}{\mathrm{Pr}}\varepsilon {y_7}^2-\frac{\mathrm{Ec}}{1+\delta y_6}\left(\frac{1}{4}{y_3}^2+{y_5}^2\right)\right], \tag{34}$$

$$y_8' = y_9\,, \tag{35}$$

$$y_9' = \mathrm{Sc}\left[s\left(\frac{\eta}{2}y_9+2y_8\right)-\frac{1}{2}y_2y_8+y_1y_9\right]-\mathrm{ScSr}\left[\frac{3Rd\mathrm{Pr}}{3Rd(1+\varepsilon y(6)-\mathrm{PrSrScDu})+4}\left\{2s(y_6-\mathrm{DuScy}_8)+\frac{\eta s}{2}(y_7-\mathrm{DuScy}_9)+\frac{1}{2}y_2(\mathrm{DuScy}_8-y_6)+y_1(y_7-\mathrm{DuScy}_9)-\frac{1}{\mathrm{Pr}}\varepsilon {y_7}^2-\frac{\mathrm{Ec}}{1+\delta y_6}\left(\frac{1}{4}{y_3}^2+{y_5}^2\right)\right\}\right] \tag{36}$$

with boundary conditions:

– at η =0:

$$y_1 = f_w\,, \quad y_2 = 0, \quad y_4 = 1, \quad y_8 = 1, \tag{37a}$$

– as $\eta \to \infty$:

$$y_2 = 0, \quad y_4 = 0, \quad y_6 = 0, \quad y_8 = 0. \tag{37b}$$

4. Results and discussion

The outcomes are analysed using numerical computations for a variety of parameter values. In order to facilitate the investigation, the values assigned to Pr and Sc are taken into consideration for an electrically conducting fluid, namely metal ammonia suspensions (Pr = 0.78), contaminated by water vapour (Sc = 0.6). All the displayed figures are plotted for the fixed value of the parameter unless stated otherwise: Ri = 1; M = 1; N = 1; δ = –0.3; η = 0.1; Pr = 0.78; ε = 0.3; Rd = 0.2; Ec = 0.01; Du = 0.3; Sc = 0.6; Sr = 0.5; f_w = 0.1; s = 1.

Upon considering the steady state flow s = 0, and under the absence of Ri, Rd, Ec, Sr, Du and at constant wall temperature with constant δ and ε, the current results are compared to the previous results obtained by Sparrow and Cess [3], Chamkha and Rashad [15] as shown in Fig. 2, in order to determine the numerical method's reliability. Table 1 also shows a comparison of numerical values of heat transfer rate $-\theta'(0)$ by taking varying values of Pr, Ri with those obtained in the study conducted by Chamkha and Rashad [15] and Malik et al. [30]. Thus, the results plotted in Fig. 2 and the numerical data presented in Table 2 show that the results obtained using the current method are accurate and hence justify the reliability of the study conducted.

The outcomes of the ascending viscosity parameter δ are sketched in Figs. 3–6. As the fluid becomes more viscous the resistance to flow increments and thus the tangential and azimuthal velocities of the fluid are found to decrease; but an opposite trend on the tangential velocity of the fluid near the conical surface is also important to note in the current study. From Fig. 3 it is detected that the tangential velocity experiences a significant rise within the region $0 \le \eta < 1.7$ which then continues to deplete beyond $\eta > 1.7$. Hence it can be deduced that δ generates an escalation in the tangential velocity near the conical surface while producing a drop in velocity towards the edge of the boundary layer. The tangential and azimuthal skin friction improves by about 8.9% and 8.3%, respectively, when δ varies from –0.3 to –0.2 (see Table 2). Furthermore, as the viscosity of the fluid increases the interactions between particles decrease, and hence the temperature and solutal profiles gradually decay (see Fig. 5, Fig. 6), which weakens the thermal and solutal boundary layer thickness. The heat and mass transfer rates undergo growth by about 0.3% each when δ varies from –0.3 to –0.2 (see Table 2).

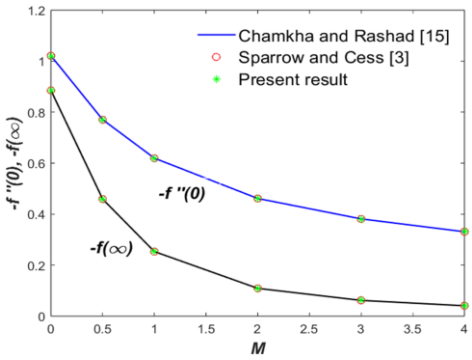

Fig. 2(a). Numerical results obtained for $-f''(0)$ and $-f(\infty)$ are compared for ascending values of M.

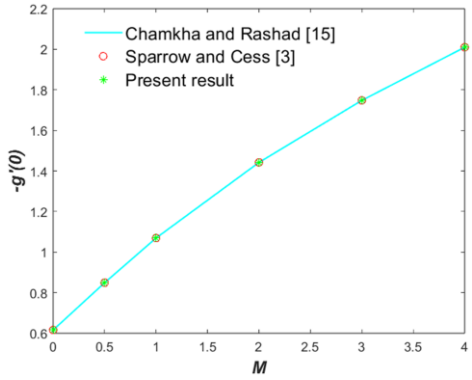

Fig. 2(b). Numerical results obtained for $-g'(0)$ are compared for ascending values of M.

Table 1. Numerical values of $-\theta'(0)$ compared for varying Pr, Ri.

Pr	Present Result			Malik et al. [30]			Chamkha and Rashad [15]		
	Ri			Ri			Ri		
	0	1	10	0	1	10	0	1	10
0.7	0.4291	0.6120	1.0173	0.4295	0.6121	1.0097	0.4299	0.6120	1.0097
10	1.4083	1.6076	2.3535	1.4110	1.5660	2.3581	1.4110	1.5662	2.3580

Table 2. Numerical values for the tangential $-f''(0)$ and azimuthal skin frictions $-g'(0)$, heat transfer rate $-\theta'(0)$ and the mass transfer rate $-\phi'(0)$.

δ	M	ε	Pr	Rd	Ec	Du	Sr	Sc	s	$-f''(0)$	$-g'(0)$	$-\theta'(0)$	$-\varphi'(0)$
–0.3	1	0.3	0.78	0.2	0.01	0.3	0.5	0.6	1	1.69556	1.22616	0.45051	1.10591
–0.2										1.84638	1.32767	0.45164	1.10969
	1.5									1.59682	1.33891	0.44650	1.09859
		0.5								1.69779	1.22684	0.44348	1.10728
			1							1.67406	1.21989	0.50553	1.09636
				0.4						1.64781	1.21217	0.57606	1.08379
					0.1					1.69701	1.22662	0.44200	1.10799
						0.5				1.69985	1.22747	0.43568	1.10894
							0.7			1.69949	1.22661	0.45107	1.09271
								1		1.64238	1.22090	0.44055	1.39664
									1.5	1.52572	1.31805	0.53074	1.30816

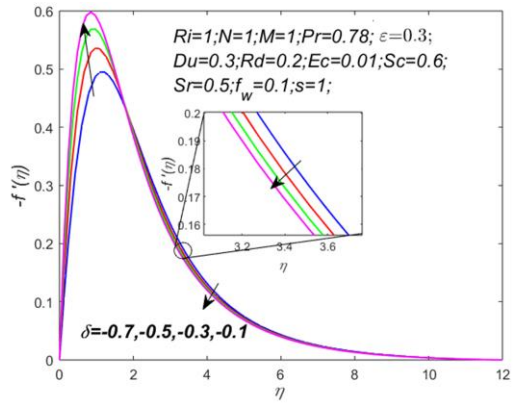

Fig. 3. $-f'(\eta)$ profiles for ascending δ.

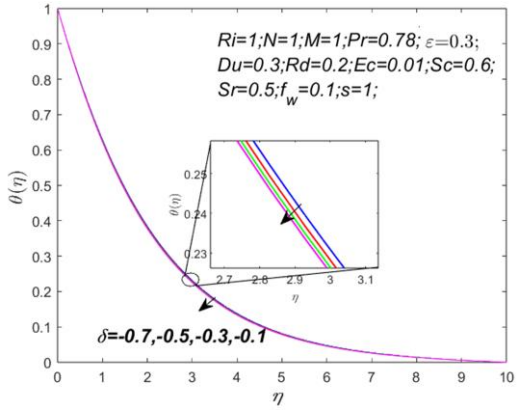

Fig. 5. $\theta(\eta)$ profiles for varying δ.

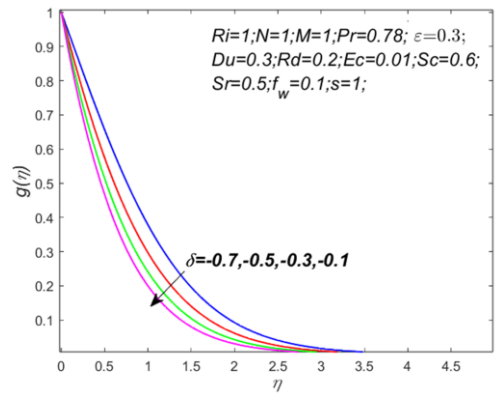

Fig. 4. $g(\eta)$ profiles for ascending δ.

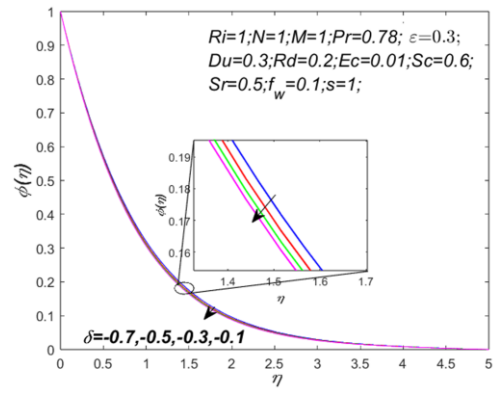

Fig. 6. $\phi(\eta)$ profiles for ascending δ.

Figures 7–8 exemplify that as the magnetic parameter M surges, the tangential and azimuthal velocities of the fluid decrease drastically. These results are due to the existence of Lorentz force which is a resistive force that occurs in the azimuthal direction when an electrically conducting fluid is exposed to a transverse magnetic field. Hence, the motion of the fluid is retarded by this force. Consequently, from Table 2 a draining effect on the tangential skin friction, heat, and mass transfer rates by about 5.8%, 0.9%, and 0.7%, respectively, is observed, while the azimuthal skin friction improves up to 9.2% when M is increased from 1.0 to 1.5.

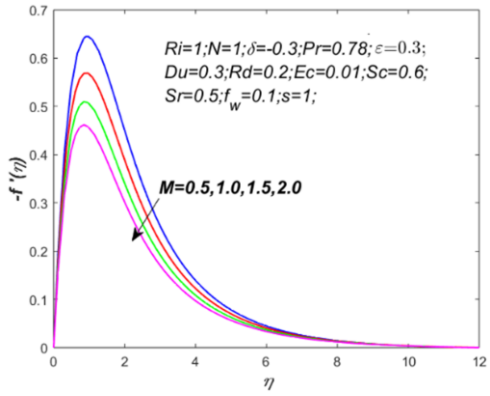

Fig. 7. $-f'(\eta)$ profiles for ascending M.

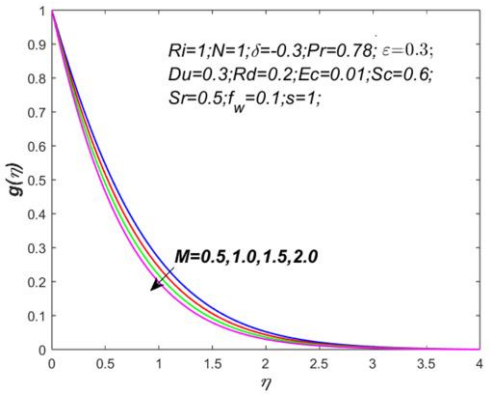

Fig. 8. $g(\eta)$ profiles for ascending M.

Figure 9 gives an estimation of the effect of ascending Prandtl number Pr accounted for air (0.72), electrolytic solution (1.00), water (7.00), and water at 4°C (11.40) on the temperature profile. In the figure, a decreasing trend in the temperature profile is observed. This result can be justified by the fact that higher Pr denotes lower thermal diffusivity, and thus the higher the fluid's Pr value the lower the temperature. From Table 2 it can be concluded that the tangential and azimuthal skin frictions along with the mass transfer rate diminish by about 1.3%, 0.5% and 0.9%, respectively, while the heat transit rate goes up to 12.2% when Pr varies from 0.78 and 1.00. Hence according to the results obtained, it can be said that fluids with lower Pr have higher thermal conductivities, allowing heat to flow more efficiently from the surface of the cone than fluids with higher. Thus, the cooling rate in the conducting fluid can be influenced by Pr.

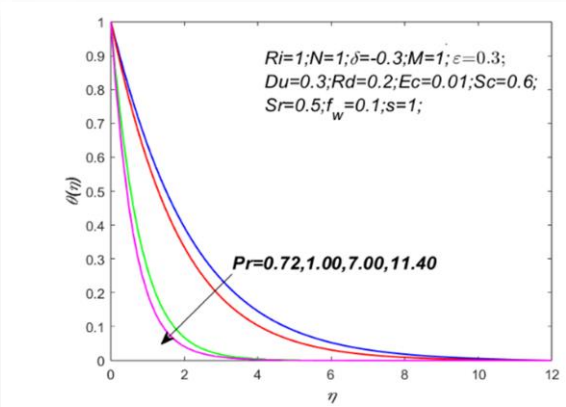

Fig. 9. $\theta(\eta)$ profiles for ascending Pr.

Figures 10–11 are plotted to depict the influence of temperature dependent thermal conductivity ε on the tangential velocity and temperature. Thermal conductivity improves the tangential velocity of the fluid and the ability to conduct heat increments which eventually improve the thermal boundary layer thickness.

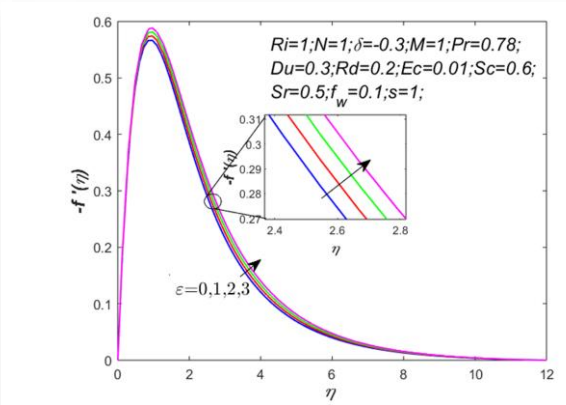

Fig. 10. $-f'(\eta)$ profiles for ascending ε.

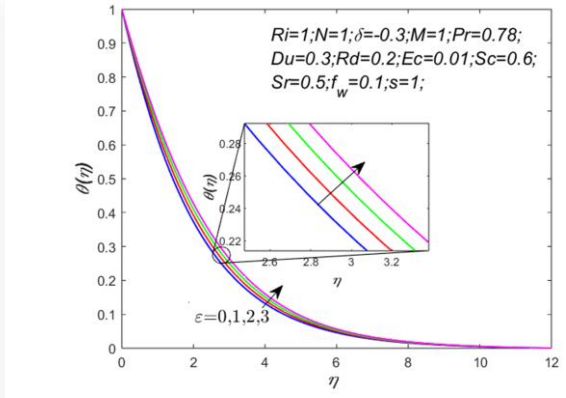

Fig. 11. $\theta(\eta)$ profiles for ascending ε.

From the result plotted in Fig. 10, it can also be deduced that the tangential velocity of the fluid near the conical surface re-

mains unaffected by ascending values of ε but gradually grows at a distance away from the conical surface. The tangential skin friction is found to undergo a growth up to 0.1% while the heat transfer rate degrades by about 1.6%; for ε varying from 0.3 to 0.5 (see Table 2).

The effect of Eckert (Ec) number on the tangential velocity and temperature profiles is presented in Figures 12–13. The Ec number is directly related to kinetic energy; increasing Ec directly leads to enhancement of the fluid's kinetic energy which consequently leads to the improvement of the fluid's tangential velocity and thickening of the thermal boundary layer. Moreover, from Fig. 12 it can be concluded that at the region near the conical surface, the effect of ascending Ec is equivalent to zero, however at a certain range of about $\eta > 0.5$ the change in pattern on the tangential velocity can be detected. According to findings reported in Table 2, varying Ec from 0.01 to 0.10 causes the heat transfer rate to be reduced by about 1.9%.

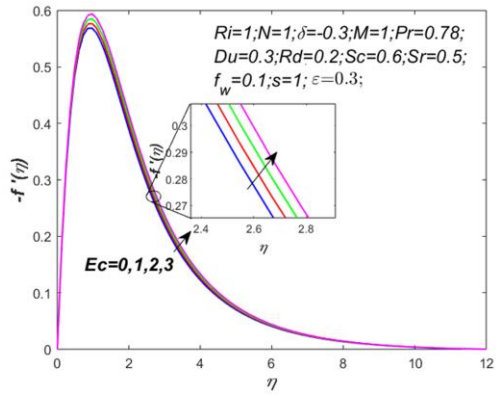

Fig. 12. $-f'(\eta)$ profiles for ascending Ec.

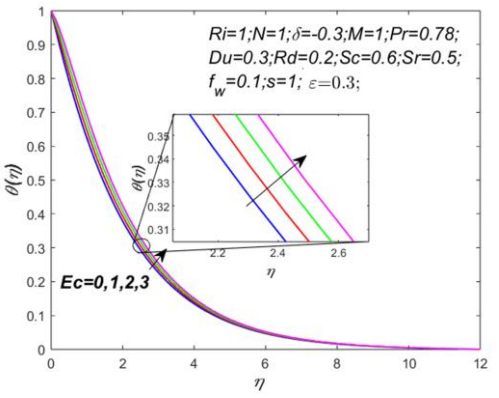

Fig. 13. $\theta(\eta)$ profiles for ascending Ec.

Figure 14 gives an illustration of the tangential velocity distribution of the fluid for ascending values of both the Soret (Sr) and Dufour (Du) numbers. As the temperature and mass flux in the fluid continuously increase, the tangential velocity profile is also found to be consequently increased. An illustration of the effect of Du on the temperature profile is found in Fig. 15; according to the illustration, the temperature profile undergoes a certain boost as Du increases. This is because at the boundary flow region, the kinematic viscosity starts to decrease as Du increases and thus the fluid's kinetic energy improves which consequently leads to the acceleration of the fluid and enhancement of the temperature profile. The influence of ascending Sr on the solutal profile is plotted in Fig. 16. The figure depicts that the solutal profile undergoes growth as Sr improves. This is because a higher Sr corresponds to a higher temperature gradient which consequently leads to higher convective flow and thus results in thickening of the concentration boundary layer.

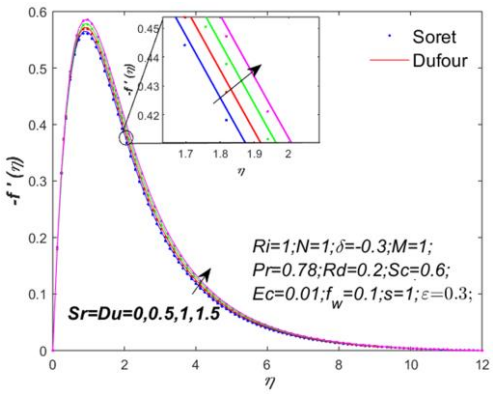

Fig. 14. $-f'(\eta)$ profiles for ascending Du, Sr.

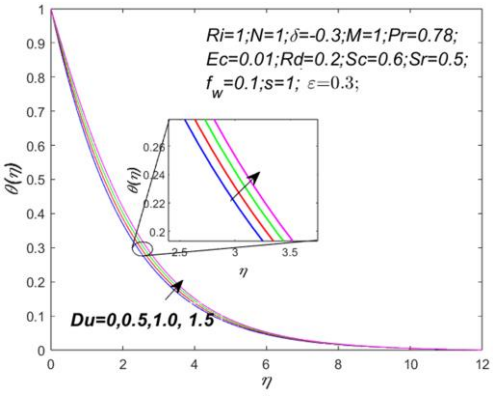

Fig. 15. $\theta(\eta)$ profiles for ascending Du.

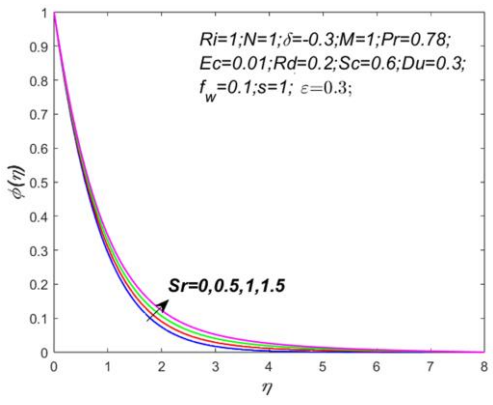

Fig. 16. $\phi(\eta)$ profiles for ascending Sr.

According to results shown in Table 2, it is certain that higher Du inflicts around a 3.3% drop in the heat transfer rate and higher Sr inflicts around a 1.2% drop in the mass transfer rate within the range of $0.3 \le Du \le 0.5$ and $0.5 \le Sr \le 0.7$.

Figure 17 gives an estimated graph showing the influence of ascending Schmidt (Sc) number plotted for hydrogen (0.22), water vapour (0.62), ammonia at 25°C (0.78), and CO_2 at 25°C (1.00). It is determined that the decline in concentration becomes more substantial for heavier species. This decrease in the solutal profile is further supported by the fact that Sc and species diffusivity are inversely related to each other. Thus, higher Sc implies lower species diffusivity, which consequently leads to depletion of the solutal profile. Results in Table 2 show that as Sc enhances from 0.6 to 1.0, the mass transfer rate improves up to 26.3% and deteriorates the tangential skin friction and the heat transfer rate around 3.2%, and 2.2%, respectively. Hence, the greater the mass transfer rate, the lower the fluid concentration boundary layer.

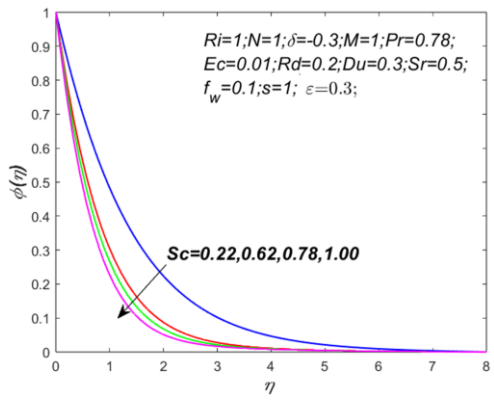

Fig. 17. $\phi(\eta)$ profiles for ascending Sc.

Results are presented for the tangential velocity, temperature, and solutal profiles in Figs. 18–20 for the ascending unsteady parameter s.

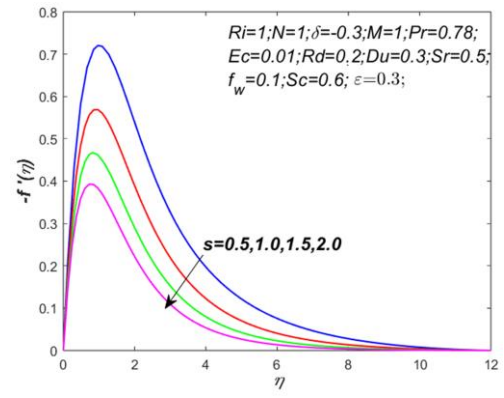

Fig. 18. $-f'(\eta)$ profiles for ascending s.

It is certain from the figures that ascending s leads to the decrement of the tangential velocity as well as the temperature and solutal profiles. Thus, it can be deduced that the rate of cooling becomes much faster in unsteady state flow as compared to those in steady flow. Also, mass transfer takes place at a slower pace in unsteady flows as compared to steady flows.

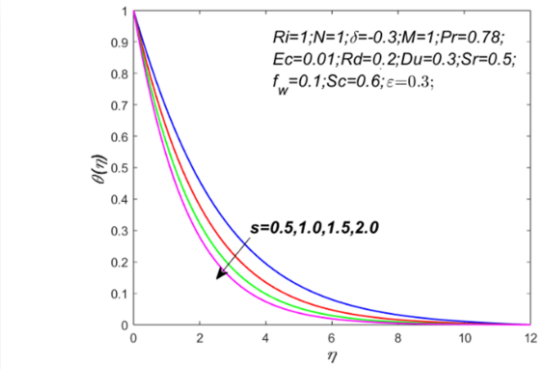

Fig. 19. $\theta(\eta)$ profiles for ascending s.

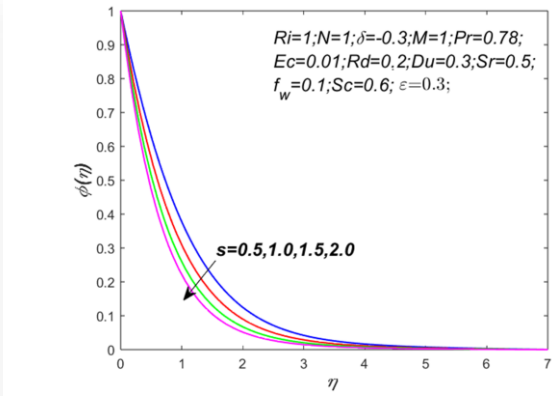

Fig. 20. $\phi(\eta)$ profiles for ascending s.

According to Table 2, it can be established that the tangential skin friction decreases significantly by about 10%, while leading to enhancement in the azimuthal skin friction, heat, and mass transfer rates by a significant percentage up to 7.5%, 17.8%, and 18.3%, respectively, as s varies from 1 to 1.5.

5. Conclusions

The study has been conducted to understand and numerically analyze the effects of the temperature dependent viscosity and thermal conductivity, viscous dissipation, and the Soret and Dufour effects on the boundary layers for the unsteady permeable rotating cone. The following are some of the conclusions that can be made regarding the problem under consideration:

The viscosity parameter δ has an opposite effect on the tangential velocity $-f'(\eta)$, i.e. near the surface of the cone the tangential velocity $-f'(\eta)$ increases, and away from the conical surface, the tangential velocity $-f'(\eta)$ decreases.

The growth of viscosity parameter δ reduces the azimuthal velocity $g(\eta)$, temperature $\theta(\eta)$ and concentration $\phi(\eta)$ profiles.

In the presence of a magnetic field, the Lorentz force acts to reduce the tangential velocity $-f'(\eta)$ and the azimuthal velocity $g(\eta)$ profiles.

With the growth in thermal conductivity ε and Eckert number Ec, the profiles of the tangential velocity $-f'(\eta)$ and the azimuthal velocity $\theta(\eta)$ grow. The increase in Dufour Du and Soret Sr numbers lead to growth of the temperature $\theta(\eta)$ and concentration $\phi(\eta)$ profiles, respectively.

If the viscosity parameter δ changes from −0.3 to −0.2 then the magnitude of the tangential skin friction $-f''(0)$ and the azimuthal skin friction $-g(0)$ increase up to 8.9% and 8.3% each. Similarly, if the unsteady parameter s increases to 1.5 from 1, then the azimuthal skin friction $-g'(0)$, the heat transfer rate $-\theta'(0)$ and the mass transfer rate $-\phi'(0)$ show 7.5%, 17.8% and 18.3% hikes, respectively.

The increment of thermal conductivity ε and Eckert number Ec from 0.3 to 0.5 and 0.01 to 0.1, respectively, causes a 1.6% and 1.9% drop in the heat transfer rate $-\theta'(0)$.

Varying Dufour Du and Soret Sr from 0.3 to 0.5 and 0.5 to 0.7, respectively, causes 3.3% and 1.2% drop-in the heat transfer rate $-\theta'(0)$ and the mass transfer rate $-\phi'(0)$. It is intended that the physics of flow across the permeable rotating cone may be used as the foundation for various engineering and scientific applications using our current model. Also, as a motivator for future experimental work, which appears to be missing now.

References

[1] Tien, C.L., & Tsuji, I.J. (1965). A theoretical analysis of laminar forced flow and heat transfer about a rotating cone. *Journal of Heat Transfer*, 87(2), 184–190. doi: 10.1115/1.3689069

[2] Hering, R.G., & Grosh, R.J. (1962). Laminar free convection from a non-isothermal cone. International Journal of Heat and Mass Transfer, 5(11), 1059–1068. doi: 10.1016/0017-9310(62)90059-5

[3] Sparrow, E.M., & Cess, R.D. (1962). Magnetohydrodynamic flow heat transfer about rotating disk. *Journal of Applied Mechanics*, 29, 181–187.

[4] Chamkha, A.J. (1996). Non-darcy hydromagnetic free convection from a cone and a wedge in porous media. *International Communications in Heat and Mass Transfer*, 23(6), 875–887. doi: 10.1016/0735-1933(96)00070-X

[5] Takhar, H.S., Chamkha, A.J., & Nath, G. (2003). Unsteady mixed convection flow from a rotating vertical cone with a magnetic field. *Heat and Mass Transfer*, 39, 297–304. doi: 10.1007/s00231-002-0400-1

[6] Ece, M. C. (1992). The initial boundary-layer flow past a translating and spinning rotational symmetric body. *Journal of Engineering Mathematics*, 26, 415–428. Doi: 10.1007/BF00042743

[7] Chamkha, A.J., & Al-mudhaf, A. (2005). Unsteady heat and mass transfer from a rotating vertical cone with a magnetic field and heat generation or absorption effects. *International Journal of Thermal Sciences*, 44, 267–276. doi: 10.1016/j.ijthermalsci.2004.06.005

[8] Anilkumar, D., & Roy, S. (2004). Unsteady mixed convection flow on a rotating cone in a rotating fluid. *Applied Mathematics and Computation*, 155(2), 545–561. doi: 10.1016/S0096-3003(03)00799-9

[9] Gorla, R.S.R., Chamkha, A.J., & Rashad, A.M. (2010). Mixed convective boundary layer flow over a vertical wedge embedded in a porous medium saturated with a nanofluid. *3rd International Conference on Thermal Issues in Emerging Technologies, Theory and Applications, Proceedings, ThETA3 2010*, 6(207), 445–451. doi: 10.1109/THETA.2010.5766429

[10] Reddy, M.G., Rani, M.V.V.N.L.S., Kumar, K.G., & Prasannakumara, B.C. (2018). Cattaneo–Christov heat flux and non-uniform heat-source/sink impacts on radiative Oldroyd-B two-phase flow across a cone/wedge. *Journal of the Brazilian Society of Mechanical Sciences and Engineering*, 40(2). doi: 10.1007/s40430-018-1033-8

[11] Gnaneswara Reddy, M., Padma, P., & Sudha Rani, M.V.V.N.L. (2019). Non-linear thermal radiative analysis on hydromagnetic nanofluid transport through a rotating cone. *International Journal of Applied and Computational Mathematics*, 5(3). doi: 10.1007/s40819-019-0654-7

[12] Saleem, S. (2021). Heat and Mass Transfer of Rotational Flow of Unsteady Third-Grade Fluid over a Rotating Cone with Buoyancy Effects. *Mathematical Problems in Engineering*, 2021. doi: 10.1155/2021/5544540

[13] Shah, Z., Alzahrani, E., Jawad, M., & Khan, U. (2020). Microstructure and Inertial Characteristics of MHD Suspended SWCNTs and MWCNTs Based Maxwell Nanofluid Flow with Bio-Convection and Entropy Generation Past a Permeable Vertical Cone. *Coatings*, 10(10), 998. doi: 10.3390/coatings10100998

[14] Krishna, M.V., Ahammad, N.A., & Chamkha, A.J. (2021). Radiative MHD flow of Casson hybrid nanofluid over an infinite exponentially accelerated vertical porous surface. *Case Studies in Thermal Engineering*, 27(7), 101229. doi: 10.1016/j.csite.2021.101229

[15] Chamkha, A.J., & Rashad, A.M. (2013). Unsteady Heat and Mass Transfer by MHD Mixed Convection Flow From a Rotating Vertical Cone With Chemical Reaction and Soret and Dufour Effects. *The Canadian Journal of Chemical Engineering*, 99, 991–10. doi: 10.1002/cjce.21894

[16] Krishna, M.V., Swarnalathamma, B.V., & Chamkha, A.J. (2019). Investigations of Soret, Joule and Hall effects on MHD rotating mixed convective flow past an infinite vertical porous plate. *Journal of Ocean Engineering and Science*, 4(3), 263–275. doi: 10.1016/j.joes.2019.05.002

[17] Yasir, M., Khan, M., & Malik, Z.U. (2023). Analysis of thermophoretic particle deposition with Soret-Dufour in a flow of fluid exhibit relaxation/retardation times effect. *International Communications in Heat and Mass Transfer*, 141, 106577. doi: 10.1016/j.icheatmasstransfer.2022.106577

[18] Gnaneswara Reddy, M. (2018). Cattaneo-Christov heat flux effect on hydromagnetic radiative Oldroyd-B liquid flow across a cone/wedge in the presence of cross-diffusion. *European Physical Journal Plus*, 133(24). doi: 10.1140/epjp/i2018-11844-0

[19] Saleem, S., Firdous, H., Nadeem, S., & Khan, A.U. (2019). Convective Heat and Mass Transfer in Magneto Walter's B Nanofluid Flow Induced by a Rotating Cone. *Arabian Journal for Science and Engineering*, 44(2), 1515–1523. doi: 10.1007/s13369-018-3598-z

[20] Nadeem, S., Khan, M.N., & Abbas, N. (2020). Transportation of slip effects on nanomaterial micropolar fluid flow over exponentially stretching. *Alexandria Engineering Journal*, 59(5), 3443−3450. doi: 10.1016/j.aej.2020.05.024

[21] Khan, S.A., Hayat, T., Khan, M.I., & Alsaedi, A. (2020). Salient features of Dufour and Soret effect in radiative MHD flow of viscous fluid by a rotating cone with entropy generation. *International Journal of Hydrogen Energy*, 45(28), 14552–14564. doi: 10.1016/j.ijhydene.2020.03.123

[22] Ghoneim, N.I., Reddy, M.G., & Megahed, A.M. (2021). Numerical solution for natural convection fluid flow along a vertical cone with variable diffusivity and wall heat and mass fluxes embedded in a porous medium. *International Journal of Modern Physics C*, 32(06), 2150074. doi: 10.1142/S0129183121500741

[23] Abd El-Aziz, M. (2007). Temperature dependent viscosity and thermal conductivity effects on combined heat and mass transfer in MHD three-dimensional flow over a stretching surface with Ohmic heating. *Meccanica*, 42(4), 375–386. doi: 10.1007/s11012-006-9051-5

[24] Lai, F.C., & Kulacki, F.A. (1990). The effect of variable viscosity on convective heat transfer along a vertical surface in a saturated porous medium. *International Journal of Heat and Mass Transfer*, 33(5), 1028–1031. doi: 10.1016/0017-9310(90)90084-8

[25] Prasad, K.V., Vajravelu, K., & Datti, P.S. (2010). The effects of variable fluid properties on the hydro-magnetic flow and heat transfer over a non-linearly stretching sheet. *International Journal of Thermal Sciences*, 49(3), 603–610. doi: 10.1016/j.ijthermalsci.2009.08.005

[26] Mukhopadhyay, S. (2009). Unsteady boundary layer flow and heat transfer past a porous stretching sheet in presence of variable viscosity and thermal diffusivity. *International Journal of Heat and Mass Transfer*, 52(21–22), 5213–5217. doi: 10.1016/j.ijheatmasstransfer.2009.04.013

[27] Khan, M.N., Nadeem, S., & Muhammad, N. (2020). Micropolar fluid flow with temperature-dependent transport properties. *Heat Transfer*, 49(4), 2375–2389. doi: 10.1002/htj.21726

[28] Khan, M.N., & Nadeem, S. (2021). A comparative study between linear and exponential stretching sheet with double stratification of a rotating Maxwell nanofluid flow. *Surfaces and Interfaces*, 22, 100886. doi: 10.1016/j.surfin.2020.100886

[29] Ahmad, S., Khan, M.N., & Nadeem, S. (2022). Unsteady three dimensional bioconvective flow of Maxwell nanofluid over an exponentially stretching sheet with variable thermal conductivity and chemical reaction. *International Journal of Ambient Energy*, 43(1), 6542–6552. doi: 10.1080/01430750.2022.2029765

[30] Malik, M.Y., Jamil, H., Salahuddin, T., Bilal, S., Rehman, K.U., & Mustafa, Z. (2016). Mixed convection dissipative viscous fluid flow over a rotating cone by way of variable viscosity and thermal conductivity. *Results in Physics*, 6, 1126–1135. doi: 10.1016/j.rinp.2016.11.027

[31] Sambath, P., Sankar, D.S., & Vishwanathan, K.K. (2020). A numerical study of dissipative chemically reactive radiative MHD flow past a vertical cone with non-uniform mass flux. *International Journal of Applied Mechanics and Engineering*, 25(1), 159–176. doi: 10.2478/ijame-2020-0011

[32] Ragulkumar, E., Palani, G., Sambath, P., & Chamkha, A.J. (2023). Dissipative MHD free convective nanofluid flow past a vertical cone under radiative chemical reaction with mass flux. *Scientific Reports*, 13(1), 1–13. doi: 10.1038/s41598-023-28702-0

[33] Khan, S.A., Hayat, T., & Alsaedi, A. (2022). Thermal conductivity performance for ternary hybrid nanomaterial subject to entropy generation. *Energy Reports*, 8, 9997–10005. doi: 10.1016/j.egyr.2022.07.149

[34] Beg, O.A., Ghosh, S., & Bég, T. (2011). *Applied Magnetofluid Dynamics: Modelling and Computation* (1st ed.). LAP Lambert Academic Publishing.

[35] Brewster, M.Q. (1992). *Thermal Radiative Transfer and Properties*. John Wiley & Sons Ltd. New York.

[36] Schlichting, H., & Gersten, K. (2017). *Boundary-Layer Theory*. (9th ed.). Springer Berlin Heidelberg. doi: 10.1007/978-3-662-52919-5

[37] Shampine, L., Kierzenka, J., & Reichelt, M. (2000). Solving boundary value problems for ordinary differential equations in MATLAB with bvp4c. *Tutorial Notes*, 75, 2751–27. https://classes.engineering.wustl.edu/che512/bvp_paper.pdf [accessed 14 Nov. 2023].